Korean J. Chem. Eng., 39(12), 3482-3496 (2022)
DOI: 10.1007/s11814-022-1205-1

pISSN: 0256-1115
eISSN: 1975-7220

New understanding of the effect of particle mass loading on the performance of a square cyclone at low and high gas temperatures

Ebrahim Hosseini†, Hossein Fatahian, and Esmaeel Fatahian

School of Aerospace Engineering, Universiti Sains Malaysia, 14300, Nibong Tebal, Penang, Malaysia
(*Received 16 March 2022 • Revised 31 May 2022 • Accepted 12 June 2022*)

Abstract−Although particle loading is often assumed to have a significant impact on fluid flow in cyclone separators, the specific effect can be confusing due to a lack of fundamental knowledge of the operating principles. The problem was addressed in this work by numerically analyzing the particle mass loading impact of different sizes on the flow within the square cyclone separator using the computational fluid dynamics (CFD) approach. This type of cyclone is an effective cleaning mechanism for high-temperature gases in a circulating fluidized bed (CFB) boiler. Therefore, it is also critical to investigate the effect of particle mass loading on gas flow at low and high temperatures, which has yet to be taken into account in the literature. Consequently, the current study focuses on this issue as a first step toward developing square cyclones by better understanding the influence of particle concentration on airflow. To describe particle flow, the Eulerian-Lagrangian technique was used to solve the unsteady Reynolds-averaged Navier-Stokes (URANS) equations. The discrete random walk (DRW) was employed to evaluate velocity fluctuations. The results demonstrated that as particle mass loading increased, the sweeping impact of enhanced larger particles caused the smaller particles to flow toward the wall region, increasing particle concentration at the wall region. The particle concentration at the bottom of the square cyclone increased 11 times when the particle mass loading increased from 6.9 to 41.7 g/m^3. As the tangential velocity of the gas increased with particle mass loading, more particles accumulated at the bottom of the conical section and remained there for an extended length of time, increasing the chances of their separation.

Keywords: Square Cyclone, Eulerian-Lagrangian, Particle Mass Loading, Temperature

INTRODUCTION

Many industrial operations, including foundry processing, chemical engineering, oil refining, petrochemicals, pharmaceuticals, agriculture, and mineral processing, involve filtering particles from an air stream to protect the environment and human health from hazardous effects. Since it is one of the pollution control equipment utilized by these process industries, cyclone separators are widely employed to separate dust from gas or for product recovery. Because of their favorable qualities such as simplicity of design, low operating costs, and high compatibility with harsh operating situations, gas cyclones have been proven to be an important particle separation mechanism [1]. They are often categorized as square or conventional [2-5]. The conventional rounded cyclone is extensively utilized in industries for CFB boilers. CFB boilers are widely used in the power generating industry, providing clean coal combustion. The large body of typical cyclones became a significant disadvantage with the growth of CFB boilers owing to the thick refractory wall needing a lengthy start-up time. The square gas cyclone can be used as an option to effectively deal with these limitations. This kind of cyclone offers several benefits over the conventional circular cyclone, including design simplicity and faster start-stop time [6-8]. A square cyclone is smaller than a cylindrical cyclone, the enhanced membrane wall arrangement minimizes the volume of the multi-phase components as well as the start and stop time, and it is effectively merged with the boiler [9,10]. However, this sort of gas cyclone has a low separation efficiency. Few studies have attempted to investigate the particle separation efficiency of square cyclones and their turbulent characteristics. For example, Venkatesh et al. [11] experimentally and numerically considered three square cyclones connected in a series arrangement. Their experimental work was done to evaluate collection efficiency and pressure drop. Their series arrangement cyclone's collecting efficiency is predicted to be 61%. The series arrangement layout reduces the pressure drop to 14.3%. Moreover, the flow pattern outcome is more consistent with the experimental data. Safikhani et al. [12] numerically analyzed particle separation efficiency of small square and round (traditional) cyclones. They reported that the pressure drop in a square gas cyclone is less than that in a cylindrical one. Fatahian et al. [13] demonstrated that incorporating a laminarizer into a conventional or square cyclone improves the particle separation efficiency. Also, Fatahian et al. [14] computationally assessed the effect of dual inverse cones on the characteristics of the cyclone separator. Their research confirmed that the dual inverse cone raises the pressure drop and collection efficiency marginally in the square cyclone. Raoufi et al. [15] studied flow in square cyclones with various outlets using a numerical technique. They determined that square cyclones had a lower pressure drop than regular cyclones. In a square cyclone, Wasilewski [10] investigated the effect of altering the vortex finder diameter and insertion length on the flow field and overall performance. They concluded that the vortex finder's geometric forms had a substantial impact on the operation of square cyclone separators. Hosseini

†To whom correspondence should be addressed.
E-mail: ebrahim.2019.hosseini@gmail.com

[16] investigated the influence of inlet shape variation on the flow field and performance in a square cyclone. Three distinct inlet configurations, namely straight, inclined, and bend inlets, were specially designed to enhance the square cyclone's low separation efficiency. He proved that, while inclined and bend inlets increased pressure drop, they improved the separation efficiency of the square cyclone. Fatahian et al. [17] used computational fluid dynamics to create unique designs for square cyclones to increase separation efficiency. When compared to the conventional square cyclone, this cyclone achieved a maximum 39.2% reduction in cut-off diameter. Venkatesh et al. [9] investigated the effectiveness of a square cyclone separator by altering five essential geometric factors. They demonstrated that the optimal square cyclone generated the best results. Fatahian et al. [5] investigated three types of vortex finders: cylindrical, convergent, and divergent. The convergent vortex finder with vortex finder diameter ratio (D_2/D_1=0.75) helps the square cyclone to gather smaller particles.

It is important to remove solid particles from hot gas in various industrial operations, such as chemical material manufacturing, cleaning the outlet gas of industrial units' chimneys, and several operations in thermal power plants [18]. By utilizing proper materials and production techniques, a cyclone separator may be applied in high-pressure, high-temperature, and corrosive gas environments. Thermo-physical properties of fluids change with temperature. As a result, the cyclone's performance is impacted by the temperature of its working fluid [18]. According to the existing literature, few studies have been done to consider the performance of cyclone separators under extreme operating conditions. Safikhani et al. [18] numerically evaluated the flow field in cyclones with five distinct wall temperature profiles. This new design was developed on the concept of expanding the vortex length to boost cyclone collection efficiency and pressure drop. They revealed that in all temperature profiles, the novel design cyclones exhibited better separation efficiency and reduced pressure drop, proving their advantages over their conventional ones. Gimbun et al. [19] explored the role of inlet temperature and velocity on cyclone pressure drop. They realized that when inlet temperature goes up, the pressure drop reduces. Karagoz and Kaya [20] analyzed the heat transfer in the cyclone separator. They proved that heat transfer from the walls started to rise as inflow velocity increased. Siadaty et al. [21] carried out a detailed examination to investigate the influence of flow and particle temperatures on cyclone efficiency. Their results indicated that by augmentation of inlet temperature, the maximum tangential velocity reduced at a specific segment by 9.93% and 6.5%, respectively. Yohana et al. [22] evaluated the influence of vortex limiter location and the insertion of a metal rod on heat transfer, flow field, and cyclone performance using the CFD approach. Their findings indicated that the vortex limiter location has a considerable impact on cyclone performance. Huang et al. [23] numerically and experimentally investigated the effect of cold air stream injection on cyclone performance at high temperatures. They found that the injection of a cold stream can be used to significantly reduce the particle deposition, although this also decreases the separation efficiency and 50% cut size. Jafarnezhad et al. [24] proposed four shapes of vortex finder of a cyclone separator, namely divergent and convergent to use instead of base one under high-temperature operating conditions. Using a convergent vortex finder instead of a base vortex finder significantly helped the cyclone collect finer particles.

However, the impact of particle mass loading on cyclone performance, particularly square cyclone performance, has received less attention. When the particle mass loading exceeds 500 g/m^3, the pressure drop across the cyclone reduces and the gas tangential velocity decreases [25-27]. The cyclone separation efficiency rises with particle mass loading due to the sweeping impacts of bigger particles and particle agglomeration within the cyclone body [25]. As the particle mass loading is between 0 and 130 g/m^3, the particle separation efficiency improves as the particle mass loading increases [28,29]. Derksen et al. [30] considered the impact of particle mass loading on the flow patterns within the cyclone numerically. The presence of solid particles reduces the swirl intensity of the gas cyclone. Moreover, the turbulence of the gas flow is remarkably damped. Huang et al. [28] investigated the influence of particle mass loading on cyclone performance experimentally and numerically. They concluded that increasing the particle mass loading raised the particles near the wall. Experimental findings showed that higher particle mass loading enhanced separation efficiency when the inlet gas velocity was low. Wan et al. [31] used the Lagrangian technique to quantitatively assess the solid concentration of different particle sizes in a cyclone separator. They revealed that the presence of solid particles greatly altered the gas flow field and the swirl was minimized as the solid loading increased.

The presented literature survey reveals that although some studies have been conducted in the area of particle mass loading on cyclone performance, a fundamental understanding of particle concentration inside the cyclone is still in its early evaluation and analytical modeling steps. More emphasis was put on cyclone design and parametric analysis than on particle behavior and gas flow characteristics. Gas flow temperature, on the other hand, caused changes in cyclone performance. It is well known that square cyclones are commonly utilized in CFB boilers, hence the working fluid seems to have a high temperature. Nonetheless, studies on this approach are still lacking, especially in elucidating the flow behavior inside the square cyclone. Under the influences on cyclone performance, particularly square cyclone separator, there is quite limited experimental and numerical data for particle mass loading. This study attempts to address this gap in the literature by providing a quantitative analysis of particle concentration and conducting a comprehensive assessment of particle mass loading and its impact on cyclone separation efficiency as well as the relation between particle mass loading and gas flow temperature. This work is the first attempt to quantitatively study the effect of particle mass loading on separation efficiency and gas flow patterns for square cyclones under both low and high temperatures gas flow.

MATHEMATICAL MODELING

1. Design of Square Cyclone

Fig. 1(a) and (b) show a schematic perspective and three-dimensional model of a square gas cyclone based on Su and Mao's [32] experimental results. Table 1 summarizes the geometrical dimensions of a square cyclone. In this study, the commercial package ANSYS-ICEM CFD was utilized to create a hexahedral grid, as de-

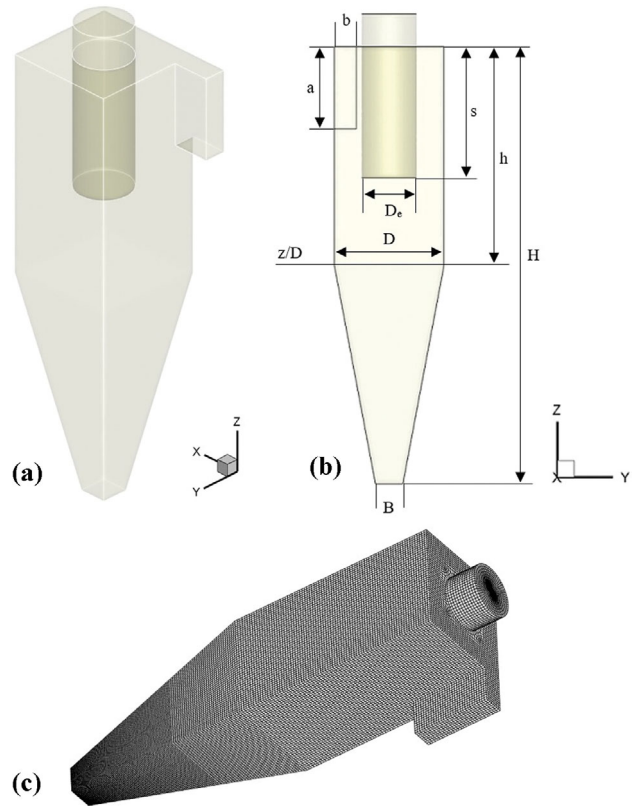

Fig. 1. Schematic view of (a) geometrical description (b) 3D model and (c) hexahedral grids.

Table 1. Cyclone dimensions (D=200 mm)

Dimensions	D_e/D	a/D	b/D	s/D	h/D	H/D	B/D
Square cyclone	0.5	0.75	0.2	1.2	2	4	0.25

picted in Fig. 1(c).

2. Governing Equations

A 3D Computational fluid dynamics simulation was done to consider the flow within the cyclone. The URANS equations for the incompressible flow can be defined as [33]:

$$\frac{\partial \overline{u}_i}{\partial x_i}=0 \tag{1}$$

$$\frac{\partial \overline{u}_i}{\partial t}+\overline{u}_j\frac{\partial \overline{u}_i}{\partial x_j}=-\frac{1}{\rho}\frac{\partial \overline{P}}{\partial x_i}+\nu\frac{\partial^2 \overline{u}_i}{\partial x_j \partial x_j}-\frac{\partial}{\partial x_j}R_{ij} \tag{2}$$

where $\overline{u}_i$ represents the mean velocity, x_i is the spatial position, ρ is the gas density, and ν is the gas kinematic viscosity. Here $\overline{P}$ shows the mean pressure and $R_{ij}=\overline{u_i'u_j'}$ is the Reynolds stress tensor, where $u_i'=u_i-\overline{u}_i$ denotes the ith fluctuating velocity component.

Only the Reynolds stress turbulence model (RSTM) and large eddy simulation (LES) are widely recognized for correctly capturing the major aspects of turbulent swirling flows of gas cyclones, according to previous studies [22,34,35]. The LES method offers more accurate findings than the RSTM for estimating the flow within cyclones, but at a higher computational cost. Hence, the RSTM [36] was utilized to analyze turbulent airflow in a square cyclone in the present CFD simulation. The RSTM computes differential transport equations for evaluating turbulence stress components, with the following turbulence production terms [36]:

$$\frac{\partial}{\partial t}R_{ij}+\overline{u}_k\frac{\partial}{\partial x_k}R_{ij}=\frac{\partial}{\partial x_k}\left(\frac{\nu_t}{\sigma^k}\frac{\partial}{\partial x_k}R_{ij}\right)-\left[R_{ik}\frac{\partial \overline{u}_j}{\partial x_k}+R_{jk}\frac{\partial \overline{u}_i}{\partial x_k}\right]$$
$$-C_1\frac{\varepsilon}{K}\left[R_{ij}-\frac{2}{3}\delta_{ij}K\right]-C_2\left[P_{ij}-\frac{2}{3}\delta_{ij}P\right]-\frac{2}{3}\delta_{ij}\varepsilon \tag{3}$$

where, P_{ij} can be defined as [31]:

$$P_{ij}=-\left[R_{ik}\frac{\partial \overline{u}_j}{\partial x_k}+R_{jk}\frac{\partial \overline{u}_i}{\partial x_k}\right],\quad P_f=\frac{1}{2}P_{ij} \tag{4}$$

with P_f is the fluctuating energy production, ν_t is the turbulent (eddy) viscosity, and σ^k=1, C_1=1.8, C_2=0.6 are empirical constants. The transport equation for turbulence dissipation rate, ε, is expressed as follows [37]:

$$\frac{\partial \varepsilon}{\partial t}+\overline{u}_j\frac{\partial \varepsilon}{\partial x_j}=\frac{\partial}{\partial x_j}\left(\left(\nu+\frac{\nu_t}{\sigma^\varepsilon}\right)\frac{\partial \varepsilon}{\partial x_j}\right)-C^{\varepsilon 1}\frac{\varepsilon}{K}R_{ij}\frac{\partial \overline{u}_i}{\partial x_j}-C^{\varepsilon 2}\frac{\varepsilon^2}{K} \tag{5}$$

$K=\frac{1}{2}\overline{u_i'u_i'}$ is the fluctuating kinetic energy, and ε is the turbulence dissipation rate. The values of constants are σ^ε=1.3, $C^{\varepsilon 1}$=1.44, $C^{\varepsilon 2}$=1.92.

The CFD code Ansys Fluent 2021 R1 was employed to simulate the two-phase flow by using the Eulerian-Lagrangian method. By solving momentum equations, the gas phase was assumed continuous in this methodology, whereas the solid phase (discrete phase) was solved by tracking particles through the flow field [38]. Particle-particle interactions can be neglected if the dispersed second phase has a low volume fraction. Since the particle volume fraction was lower than 10^{-3} in most regions, the interaction between the particles was negligible and the two-way coupling method considering the interaction between the particles and the gas stream was used in the present study [29]. The discrete phase model (DPM) was adopted for evaluating particle trajectories in a Lagrangian reference frame by characterizing the density and size of individual particles [11,33].

The stochastic tracking model may predict particle dispersion due to turbulence in the fluid phase. Through the adoption of stochastic methods, the stochastic tracking model incorporates the influence of instantaneous turbulent velocity fluctuations on particle trajectories [21,39]. In the present CFD simulation, to evaluate turbulent particle dispersion, the discrete random walk (DRW) model [40] was utilized. The Rosin-Rammler equation was employed to account for the particle size distribution. Morsi and Alexander [41] correlation was applied to calculate the drag coefficient of spherical particles in terms of relative Reynolds number (Re_p).

The particle equation of motion is expressed as [42]:

$$\frac{du_{pi}}{dt}=\frac{18\mu}{\rho_p d_p^2}\frac{C_D Re_p}{24}(u_i-u_{pi})+\frac{g_i(\rho_p-\rho)}{\rho_p} \tag{6}$$

$$\frac{dx_{pi}}{dt}=u_{pi} \tag{7}$$

where the term $\frac{18\mu}{\rho_p d_p^2}\frac{C_D Re_p}{24}(u_i-u_{pi})$ denotes the drag force per

unit particle mass.

In Eq. (6), ρ_p and d_p indicate the particle density and diameter, respectively, C_D is the drag coefficient, u_i and u_{pi} represent the instantaneous gas and particle velocities, respectively. g_i is the gravitational acceleration and Re_p is the relative Reynolds number, which is described as:

$$Re_p = \frac{\rho_p d_p |u - u_p|}{\mu} \quad (8)$$

where μ denotes the dynamic viscosity.

3. Solver Setting and Boundary Conditions

The finite volumes method (CFD code Ansys Fluent 2021 R1) was employed to numerically solve the governing equations of gas flow. The current CFD simulation began with the steady solver (gas only) for 10000 iterations and then shifted to an unsteady solver (particle tracking) with a time step of 10^{-4} seconds with the particle feeding inflow time from 0.5 s to 1.0 s. The total simulation flow time was 3.5 s for efficiency calculations. The results provided for particle motion were the data analyzed at flow times between 1.2 s to 2.0 s (from 22000 iterations to 30000 iterations).

The residence time was affected by cyclone volume and the volumetric flow rate of the gas [43]. The influence of turbulence was investigated using the RSTM and a standard wall function based on the strong swirl flow in a gas cyclone [11,17,44,45]. The case was modeled in which 10000 Fly ash particles with a density of 1,989.7 kg/m^3 were injected into the square cyclone from the inlet surface with a size distribution of 1 to 32 μm from a coal-fired boiler in a power plant. Table 2 provides the solver settings implemented in the present study.

At the gas inlet segment, the inlet velocity boundary condition was specified, and it was assumed that the particle and inlet velocity of gas were equal. The inflow velocity varied from 12 to 28 m/s. The hydraulic diameter was set to 0.0857 m and the turbulence intensity was set to 4% [33,45,46]. The outflow was assumed for the gas exit. Furthermore, the cyclone walls had a no-slip condition, and the dust outlet segment was adjusted to trap the DPM condition. Table 3 presents details of thermo-physical parameters of the gas phase (air), including viscosity and density at low and high temperatures. The temperature data were selected to match the ranges of temperature, which is reported in previous studies [21,45,47,48]. Heat transfer was not solved in the present study, and the gas flow was assumed to be isothermal but at different temperatures. On the other hand, the effect of temperature-dependence of gas thermo-physical properties on the performance of gas cyclones was analyzed. In addition, six different particle mass loadings were selected with the inflow velocities of 12 m/s and 20 m/s, as presented in Table 4.

Table 2. Solver settings

Model conditions	Model settings
Flow	Unsteady
Turbulence	RSTM
Solution method	Pressure-velocity coupling: SIMPLEC
	Spatial discretization: Pressure: PRESTO! Momentum: Quick Turbulent kinetic energy: Second-order upwind Specific dissipation rate: Second-order upwind Reynolds stresses: First-order upwind
Convergence criteria	All equations are set as 10^{-5}

Table 3. Thermo-physical properties [21,45,47,48]

T (K)	ρ (kg/m^3)	$\mu \times 10^5$ (Pa·s)
293	1.188	1.7894
700	0.4975	3.388

Table 4. Particle mass loadings considered in the present study

	Velocity	Particle mass flow rate (g/min)		
		30	90	180
Mass loading (g/m^3)	12 m/s	6.9	20.8	41.7
	20 m/s	4.2	12.5	25.0

According to previous studies [21,24,47,48], the most common range of tested temperatures is between 293 K to 700 K. Jafarnezhad et al. [24] investigated the effect of inlet temperature (T=293 K, 350 K, 500 K, and 700 K) on cyclone performance. Increasing inlet temperature significantly decreased the tangential velocity, leading to a severe reduction in the separation efficiency of the cyclone. In another study, Siadaty et al. [21] numerically investigated the performance parameters of two Stairmand high-efficiency cyclones (one with a single inlet and another with double inlets). Their results showed that by increasing inlet temperature from 293 to 700 K, the maximum tangential velocity at a specified section at the inlet velocity of 23.85 m/s, was decreased by 9.93% and 6.5%. From the literature review, it can be concluded that two temperatures (293 K and 700 K) are the most critical values in designing the cyclone separators. Thus, we selected the minimum (T=293 K) and maximum (T=700 K) temperatures to study the effect of particle mass loading on separation efficiency and gas flow patterns for square cyclones under both low and high temperatures.

4. Grid Independence Study

The proper grid resolution is crucial to reveal the reliability of the numerical simulation. To verify the grid independence study, three different grid levels were adopted. In the first case, a coarse-type mesh was produced which contains 480,000 elements. In the second case, a medium-type with 720,000 elements was developed. In the third case, a fine-type mesh with 1,080,000 elements was generated. Following that, Fig. 2 illustrates the pressure profiles for three different meshes at z/D=0.75. The computational results confirmed mesh independence since the pressure difference between two subsequent meshes was less than 1%. As a result, for all subsequent numerical simulations, a grid with 720,000 cells (medium mesh) was utilized. This mesh achieved a fair computational cost while maintaining a sufficient amount of grid independence.

5. Validation Section

To gain confidence in the simulation, the results must be compared to existing numerical or experimental studies. The refinement

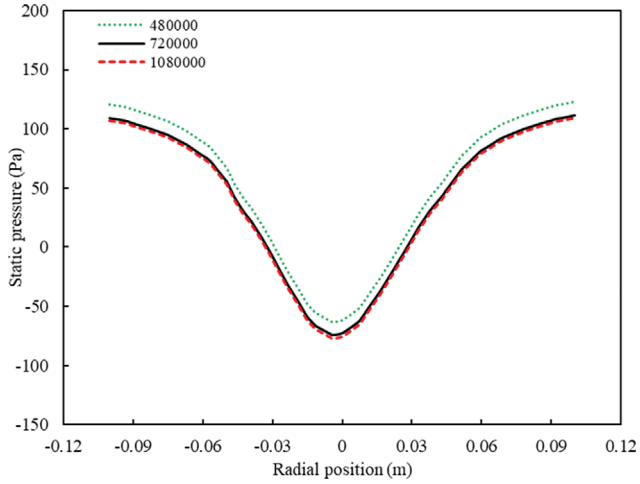

Fig. 2. Radial static pressure profiles at v=12 m/s.

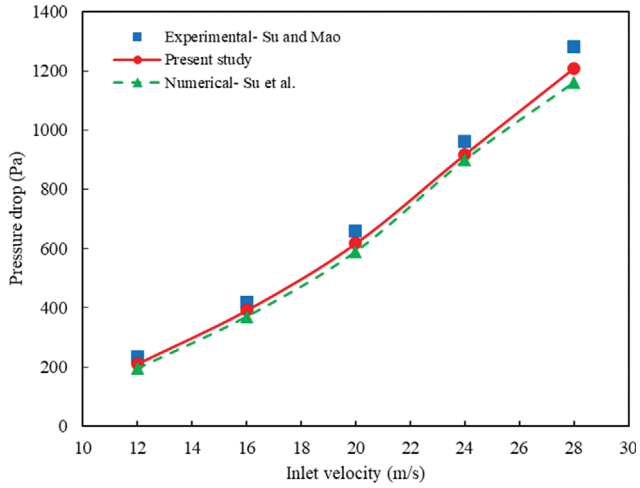

Fig. 3. Comparing the pressure drop with refs. [3,25].

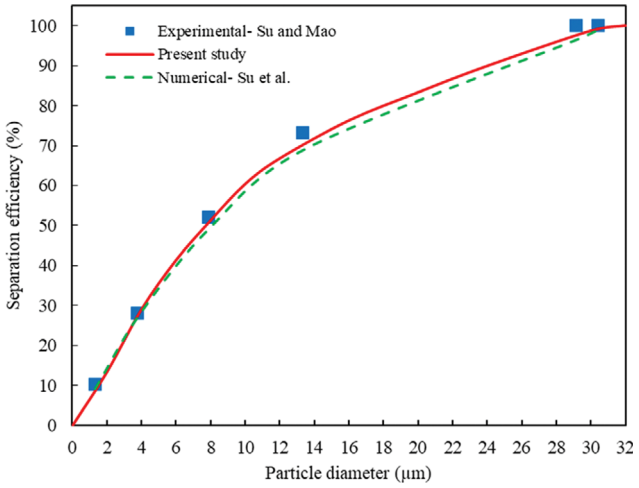

Fig. 4. Comparing the separation efficiency with refs. [3,25] at v= 20 m/s.

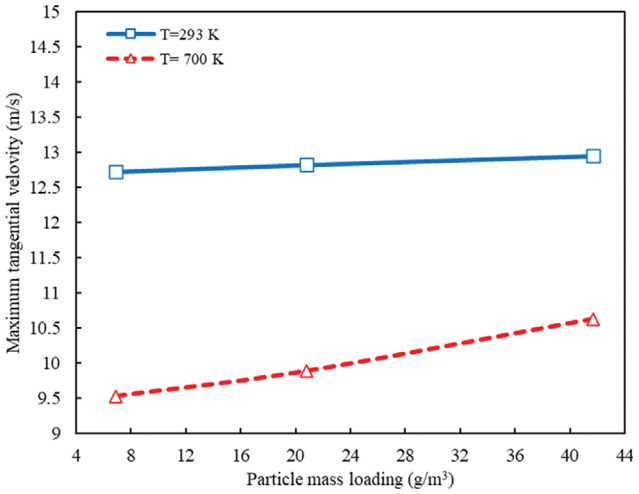

Fig. 5. Changes in the maximum tangential velocity with the particle mass loading.

ratio for mesh validation is 0.9963, which is close to unity. As a consequence, the grid has been adequately refined, the results are in the asymptotic range, and the results are independent of the number of cells. To validate the current computational model, the results were compared with the experimental study done by Su and Mao [25] and the numerical results of Su et al. [3] for the square cyclone depicted in Figs. 3 and 4. The condition of CFD modeling was chosen to be similar to those utilized in previous studies [3,25]. The present finding agrees well with the experimental data and numerical results published in previous works. The difference is less than 8%, which is within an acceptable range. This demonstrates that the present methodology quite well predicts the performance of a square cyclone in terms of separation efficiency and other parameters.

RESULTS AND DISCUSSION

1. Tangential Velocity

Fig. 5 illustrates the correlation between maximum tangential velocity and particle mass loading for a square cyclone at v=12 m/s. Note that the greatest values of tangential velocity were reported along the boundary between the inner and outer vortexes [17]. As a result, the highest tangential velocity from the time-averaged velocity field was determined at a specific spot below the vortex finder (z/D=0.75). The particle mass loading in this study was relatively low; hence, the particle impacts on the flow field were low. As demonstrated in Fig. 5, low particle mass loading resulted in a modest increase in the maximum tangential velocity. While the particle mass loading increased to 41.7 g/m^3, the increment was comparatively greater. Maximum tangential velocity increased up to 2% for particle mass loading of 41.7 g/m^3 compared to particle mass loading of 6.9 g/m^3.

Tangential velocity is an important flow characteristic because it directly influences separation efficiency and pressure drop within the cyclone. As the inlet temperature was raised, the maximum tangential velocity of all cyclones decreased dramatically. However, the increase in maximum tangential velocity owing to particle mass loading was larger at high temperatures (T=700 K) than at low gas

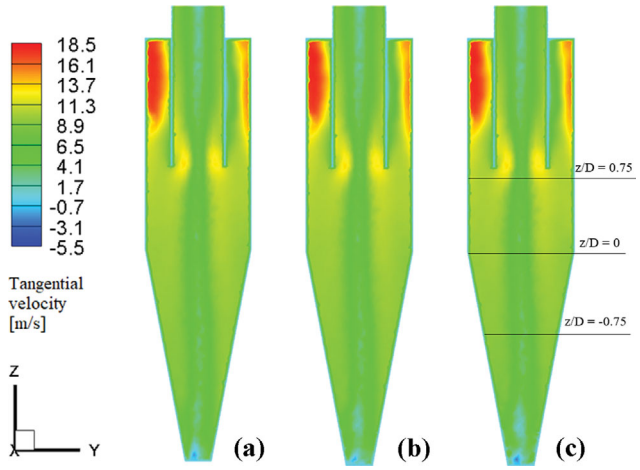

Fig. 6. Comparison of the tangential velocity contours under different particle mass loadings (a) 6.9 g/m^3 (b) 20.8 g/m^3 and (c) 41.7 g/m^3.

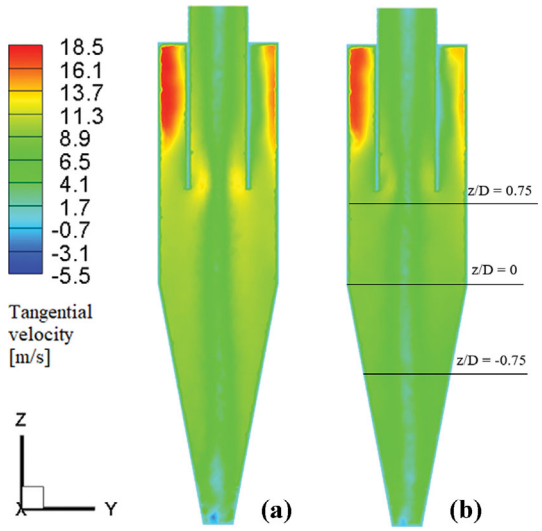

Fig. 7. Comparison of the tangential velocity contours with 41.7 g/m^3 particle mass loading at (a) T=293 K and (b) T=700 K.

temperatures. Any increase in particle mass loading contributed to an enhancement in maximum tangential velocity, especially at high temperatures. Maximum tangential velocity increased up to 12% for particle mass loading of 41.7 g/m^3 against particle mass loading of 6.9 g/m^3. Higher tangential velocity results in greater separation efficiency [49]. Consequently, the square cyclone had a lower separation efficiency at high temperatures and low particle mass loading.

Figs. 6 and 7 exhibit the tangential velocity contours for cyclones as they are affected by particle mass loading and gas temperature, respectively. The minimum and maximum gas temperatures (T= 293 K and T=700 K) were compared to assess the influence of gas temperature on tangential velocity. Three different sections from top to bottom were highlighted to analyze the velocity profiles at different separator heights. Figs. 8 and 9 demonstrate the distributions of tangential velocity for cyclone separator at v=12 m/s and

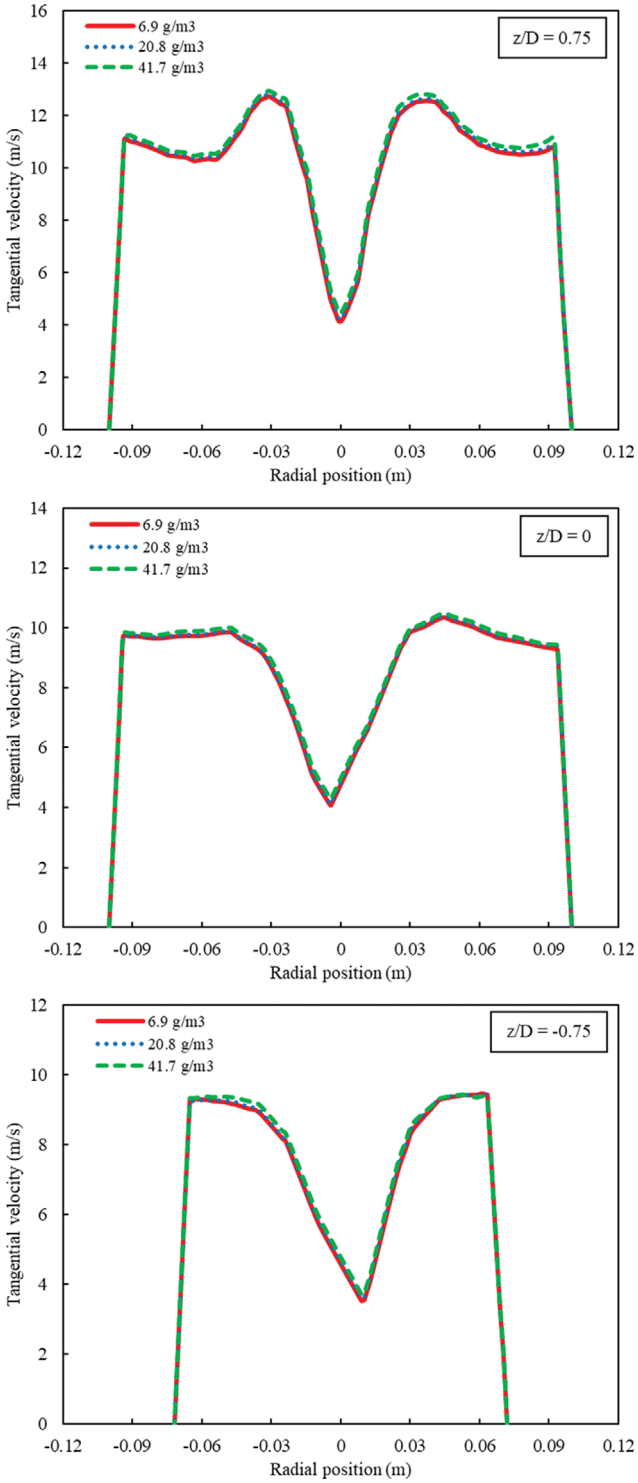

Fig. 8. Comparing the tangential velocity at different particle mass loadings.

z/D=0.75, z/D=0 and z/D=−0.75 under varying particle mass loading and different gas temperatures. The cyclone's body distribution revealed the expected forced/free Rankine-type vortex combination [50]. Tangential velocity was spread equally along the central axis of a cyclone. In addition, the greatest tangential velocity was

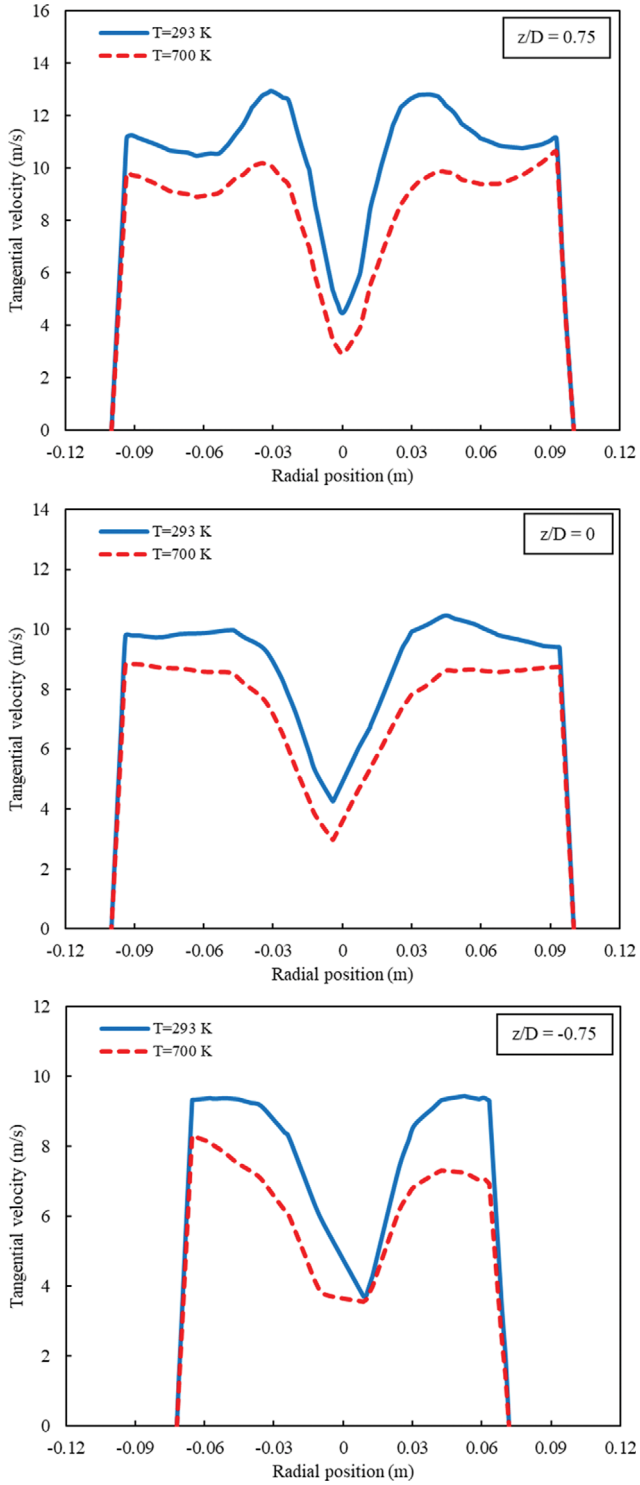

Fig. 9. Comparing the tangential velocity at different gas temperatures.

reported along the boundary between the inner and outer vortexes [17].

Comparing the velocity profile at different heights revealed that the particle mass loading variations have a minor effect on tangential velocity distributions. The profiles of tangential velocity close to the wall remained relatively constant, whereas tangential velocity profiles in the free and forced vortex zones varied significantly as particle mass loading increased, as it is observable at each height level. When the results were compared, it was noted that the tangential velocity reduced dramatically at different heights as the gas temperature increased from 293 K to 700 K. This behavior was similar to the findings of earlier investigations [24,48]. The maximum tangential velocity for the square cyclone with particle mass loading of 41.7 g/m^3 was roughly 1.1 times that of the inlet velocity at T=293 K, while it was determined to be 0.9 times that of the inlet velocity at T=700 K.

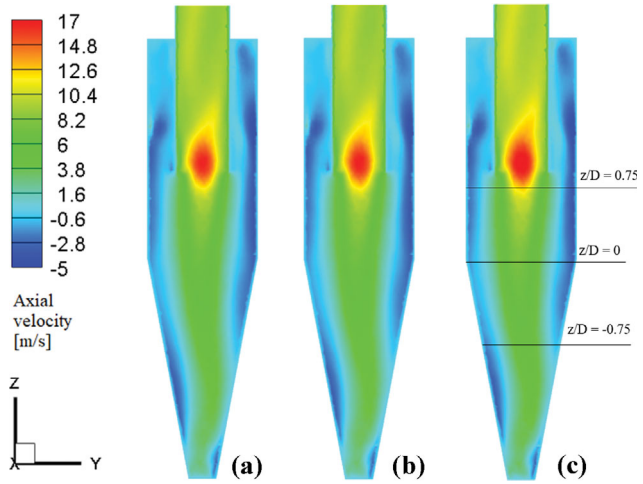

Fig. 10. Comparison of the axial velocity contours under different particle mass loadings (a) 6.9 g/m^3 (b) 20.8 g/m^3 and (c) 41.7 g/m^3.

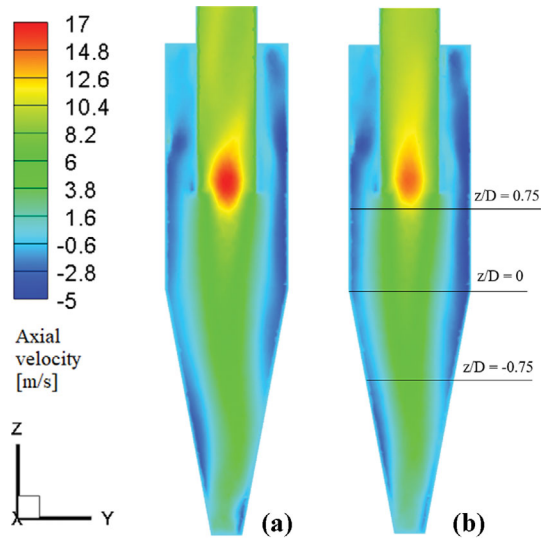

Fig. 11. Comparison of the axial velocity contours with 41.7 g/m^3 particle mass loading at (a) T=293 K and (b) T=700 K.

Figs. 10 and 11 illustrate the axial velocity contours for cyclones as they are affected by particle mass loading and gas temperature, respectively. Similar to tangential velocity contours, in these figures also three different sections were highlighted to investigate the velocity profiles at different separator heights. Figs. 12 and 13 demon-

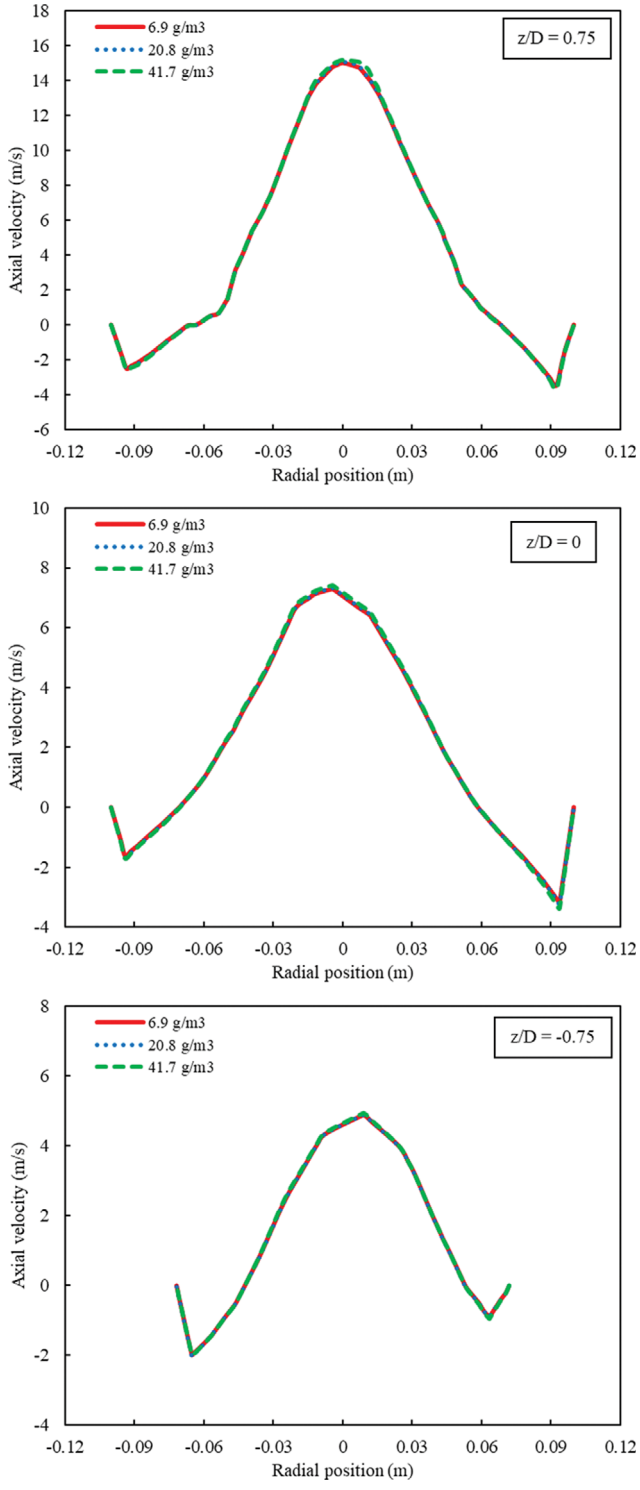

Fig. 12. Comparing the axial velocity at different particle mass loadings.

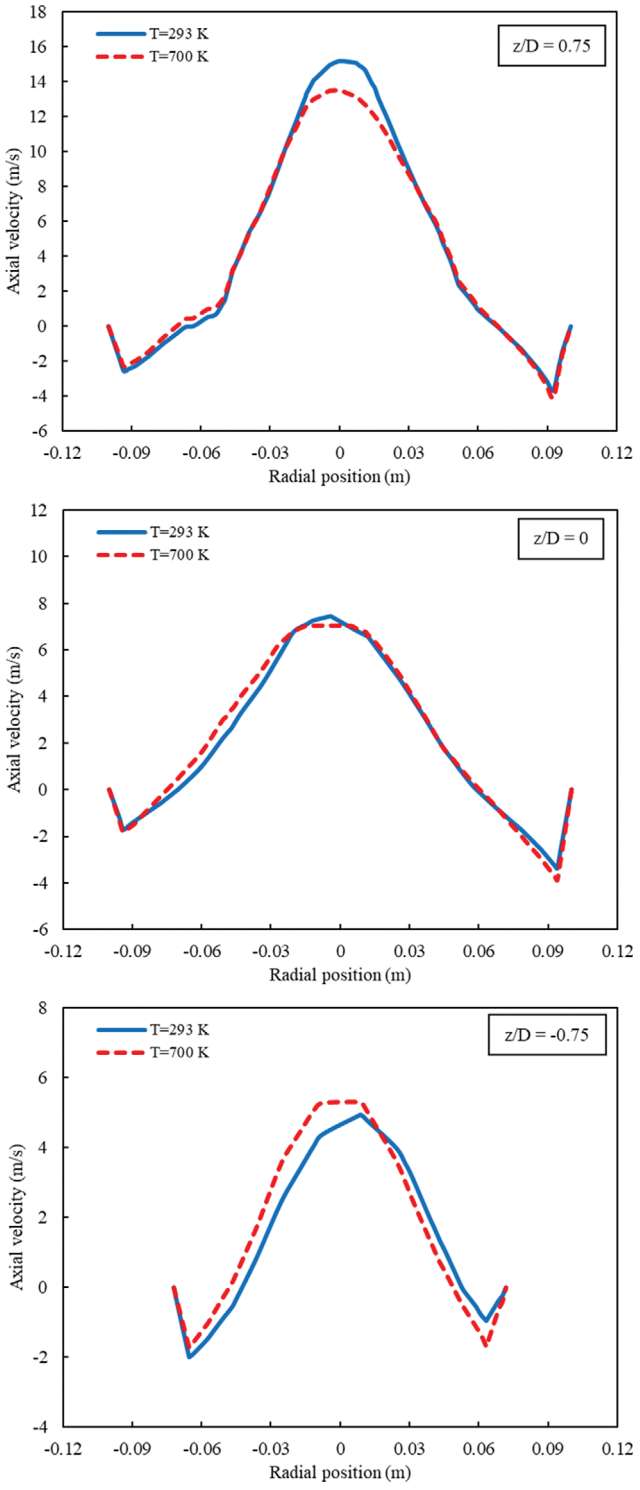

Fig. 13. Comparing the axial velocity at different gas temperatures.

strate the distributions of axial velocity for cyclone separator at v=12 m/s and z/D=0.75, z/D=0 and z/D=−0.75 under varying particle mass loading and different gas temperatures.

The highest and lowest axial velocities were commonly found at the core vortex finder and the wall, respectively. The axial velocity was negative (downward flow) at the external vortex area and grew radially inward until it reached its maximum value at the vortex core. As a result, the inverted V-pattern was seen in the axial velocity profile. Higher values of axial velocity were observed with higher particle mass loading in the region around the core where the upward gas flow has higher kinetic energy, which may overcome

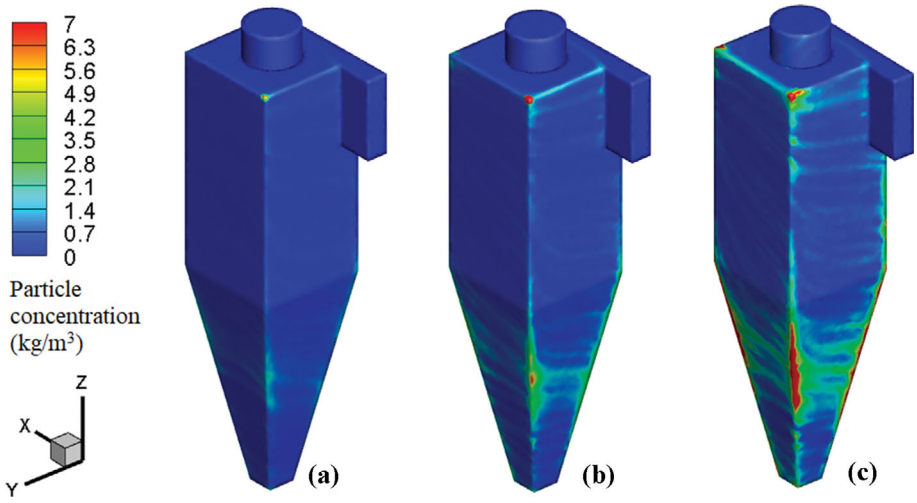

Fig. 14. Comparison of particle mass distribution in the gas cyclone under different mass loading (a) 6.9 g/m^3 (b) 20.8 g/m^3 and (c) 41.7 g/m^3.

the unfavorable pressure gradient, at z/D=0.75 (below vortex finder). On axial velocity profiles, the gas temperature was more influential than particle mass loading. When the gas temperature was increased from 293 K to 700 K, the maximum axial velocity was reduced from 15.2 m/s to 13.5 m/s at z/D=0.75. The axial velocity was greater for T=700 K at the cone section near the bottom of the cyclone, which increased the gas swirl flow and re-entrained the particles from the bottom.

2. Distribution of Particle Concentration

To assess the classification of particle concentration distribution, particle-laden simulations were performed. Fig. 14 indicates the distribution of particle concentration within the square cyclone for particle mass loading of 6.9, 20.8, and 41.7 g/m^3. This comparison was done at T=293 K and v=12 m/s at a time value of 1.4 s. The distribution of particle concentration can be classified into three categories. The particle concentration was lower in the cyclone's main section, which followed the swirling downward flow patterns of the gas. The gas tangential velocity was accelerated at the conical region of the square cyclone due to the lowering of the cone radius. The stronger centrifugal force caused by the increased tangential velocity moved particles toward the conical wall. The particle concentration was greater in the conical section of the square cyclone as the conical volume decreased and the particle numbers increased along the wall area. This pattern is more obvious in Fig. 14(c), where the particle mass loading is significantly larger than in the other. As it can be seen, as the particle mass loading increased, the particle concentration in the zone along the wall grew dramatically. Previous studies have shown that the recirculation gas flow at the top section of a cyclone with a cylindrical shape increased the concentration of larger particles and thereby a higher particle accumulation, which is known as the ceiling effect [50,51]. The accumulation of particles resulted in a greater particle accumulation near the top section of the cyclone, according to the present results.

Fig. 15 also reveals the impact of the temperature of gas on the distribution of particle concentration inside the square cyclone with particle mass loading of 41.7 g/m^3 and at v=12 m/s. It can be obviously observed that fewer particles were concentrated on the bottom part of the square cyclone at high temperatures. This is because the enhanced centrifugal force caused by increasing the gas tangential velocity was weakened, causing fewer particles to be moved toward the conical wall.

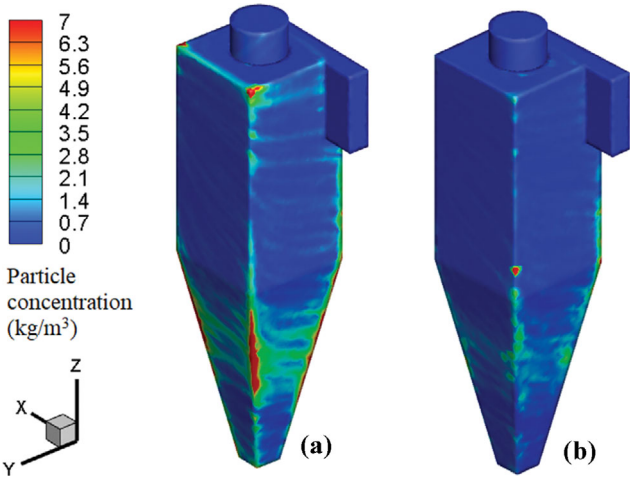

Fig. 15. Comparing the distribution of particle mass with 41.7 g/m^3 particle mass loading at (a) T=293 K and (b) T=700 K.

Fig. 16 shows the radial distribution of particle concentration at the square cyclone at z/D=0.75 (top) and z/D=−0.75 (bottom) and v=12 m/s to better explain how particles with variable mass loading behave, particularly below the vortex finder and close to the dustbin. The particle accumulation grew considerably close to the cyclone wall as a result of the inertia separation design concept. As the particle mass loading increased from 6.9 g/m^3 to 41.7 g/m^3, the particle concentration at the wall region (radial position=0.095-0.1 m) grew up to six times. As the particle mass loading increased, the improved sweeping action of the larger particles carried the smaller particles toward the wall zone, enhancing particle concentration at the wall zone [52]. The present CFD findings verified that increasing the mass loading could concentrate the particles

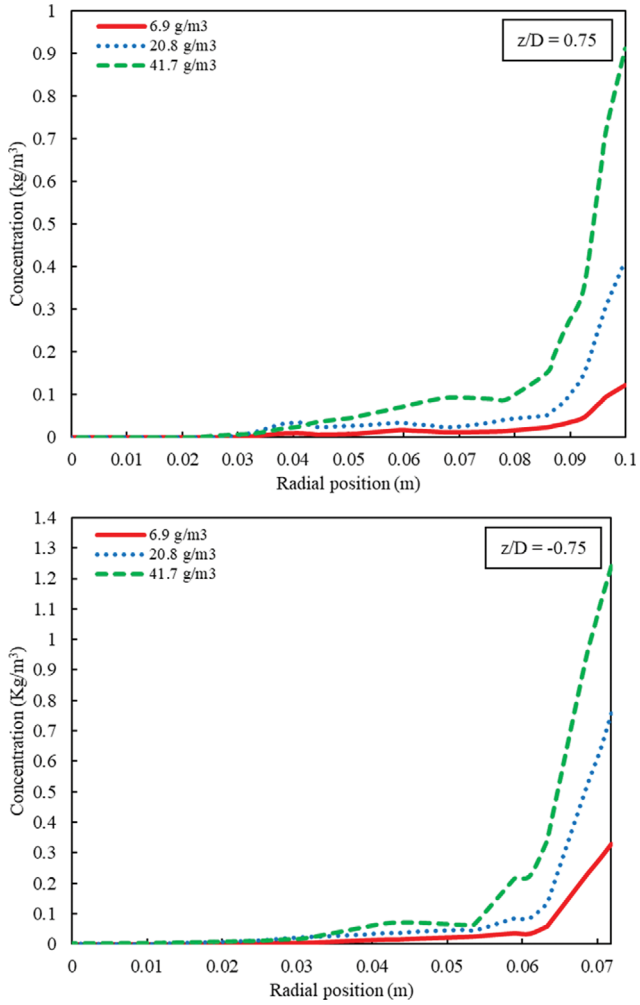

Fig. 16. Effect of particle mass loading on the distribution of particle concentration in a radial direction at T=293 K and at two levels of the separator height.

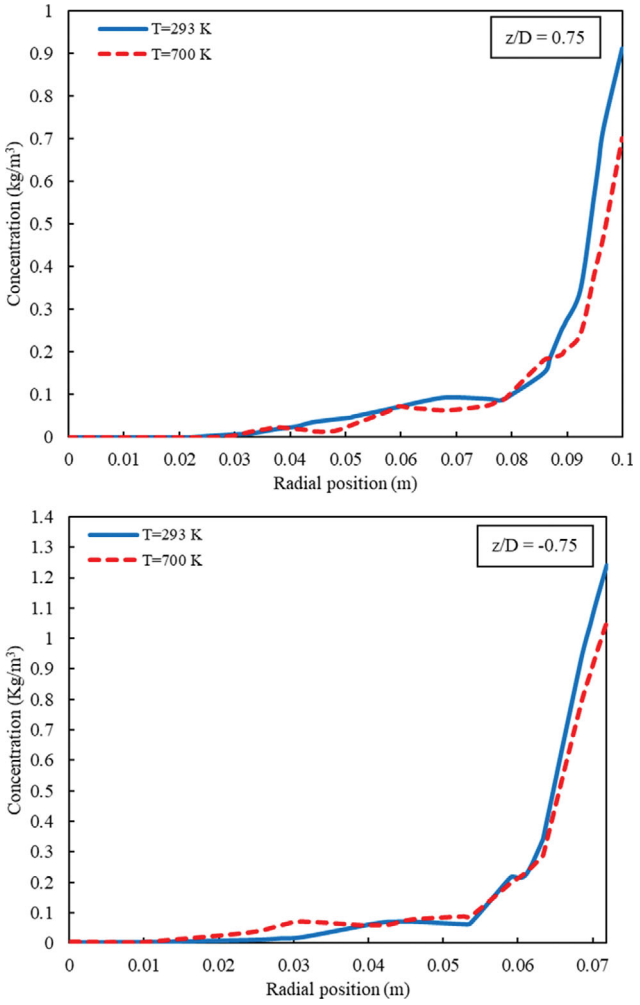

Fig. 17. Particle concentration distribution with 41.7 g/m^3 mass loading in the radial direction at two levels of the separator height.

along the wall in Fig. 16. Furthermore, comparing the considered heights confirmed that the particle concentration was higher close to the bottom as more particles were collected with larger particle mass loading.

The effect of gas temperature on the distribution of particle concentration inside a square cyclone with a particle mass loading of 41.7 g/m^3 and at v=12 m/s is shown in Fig. 17 at two levels of the separator height. The centrifugal force decreased significantly by the rise of inlet temperature, resulting in lower separation efficiency. At T=293 K, the stronger the centrifugal force, the further particles were pushed against the wall and gathered in the bottom of the cyclone (z/D=−0.75).

Fig. 18 shows the distribution of particle concentration along with the cyclone height at the centerline. The particle deposition was greater near the bottom of the square cyclone, possibly due to improved gas swirling flow patterns that developed to gradually flow downward as the particles were conveyed to the conical section. When the particle mass loading was raised from 6.9 to 41.7 g/m^3, the concentration of particles at the bottom of the square cyclone increased by up to 11 times. For low and high temperatures, Fig. 19 depicts the distribution of particle concentration at the centerline along with the height of the gas cyclone. This com-

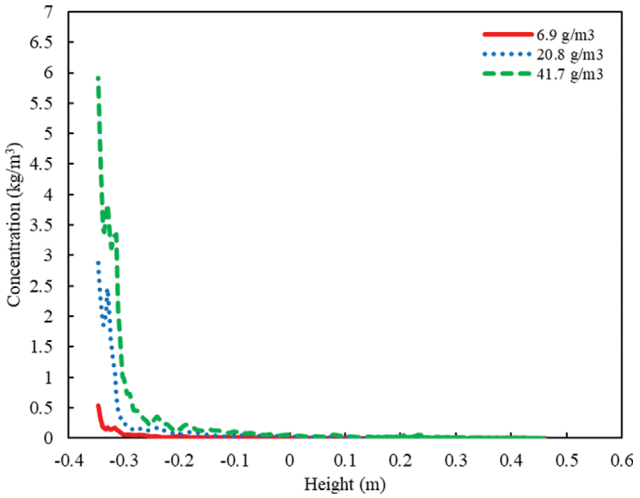

Fig. 18. Influence of particle mass loading on the distribution of particle concentration at T=293 K.

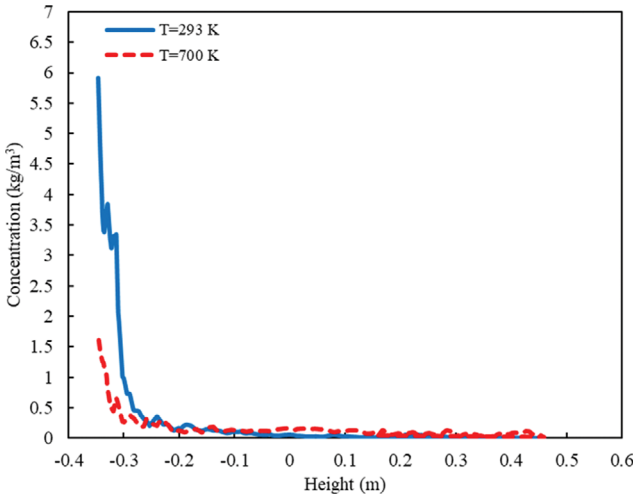

Fig. 19. Particle concentration distribution with 41.7 g/m^3 mass loading at T=293 K.

parison was done for a particle mass loading of 41.7 g/m^3 and at v=12 m/s. As discussed earlier, the tangential velocity was reduced with the increment of gas temperature. This resulted in a significant drop in particle concentration, around four times at the bottom of the square cyclone.

3. Particle Motion through the Cyclone

Fig. 20 demonstrates particle motion through a cyclone separator at v=12 m/s for a time period of 1 s at T=293 K. This figure represents the influence of particle mass loading on the motion of particle clouds with diameters ranging from 1 to 15 μm. This figure clearly shows the time evolution variations in particle motion patterns. As particles entered the square cyclone for all three particle mass loadings, they moved down to the cyclone's main body, which operated as the separating zone. The particles accumulated on the wall surface as a result of centrifugal force, as well as those collected on the bottom surface as a result of gravitational sedimentation, were separated from the gas. When the separation processes of various particles were analyzed, it was obvious that the larger particles (≥8 μm) experienced higher centrifugal force and thus were more easily separated, while most of the small particles with a diameter of 3 μm escaped through the vortex finder. The centrifugal force which acted on these small particles with a diameter of 3 μm was inadequate to eliminate gas drag force. The recirculation gas flow led larger particles to accumulate near the top of the main section of the cyclone, resulting in a greater particle concentration at this location. This was more noticeable for low particle mass loading for the first one second after entering the square cyclone. As a result, some particles were unable to be separated from the gas. Furthermore, when the gas tangential velocity increased with particle mass loading, more particles gathered at the conical bottom section and remained there for a longer time, increasing the probability of their separation.

Fig. 21 depicts the time evolution of motion particle clouds with a mass loading of 41.7 g/m^3 passing through a square cyclone with v=12 m/s at low and high temperatures. The majority of particles stayed in the center of the square cyclone's conical section. These particles were predicted to interact with the upward flow and escape from the exit section. On the contrary, the majority of the particles aggregated in the bottom of the square cyclone, while some were separated from the gas. This is because the effect of centrifugal force was stronger at T=293 K.

4. Particle Separation Efficiency

Fig. 22 illustrates the influence of particle mass loading on the particle separation efficiency of a square cyclone at two different inlet velocities (v=12 m/s and v=20 m/s). The separation efficiency was derived using the DPM model according to the collected particles in the dustbin. The efficiency improved as particle size increased, as predicted. The larger the particles, the heavier the particle collection on the wall. It was found by analyzing separation efficiencies that particle mass loading seemed to have various influences on cyclone efficiency at low and high inlet velocities. As demonstrated in Fig. 22(a), increasing the particle mass loading enhanced the cyclone separation efficiency at a lower inlet air velocity of 12 m/s. The underlying cause can be attributed to the enhancement of larger particle sweeping effects and the agglomeration of smaller particles [52]. In Fig. 22(b), the particle mass loading has less of an effect on separation efficiency for the higher velocity. The aggregation collecting process was inhibited at greater flow velocity because of the strong interaction between the smaller particle aggregations. Fig. 22(b) shows a minor increase in separation efficiency for smaller particles at greater particle mass loadings, which is most likely owing to the sweeping action of the larger particles.

As demonstrated in Fig. 23(a) and (b), the square cyclone behaved similarly at high and low gas temperatures. It is obvious that separation efficiency decreased as the temperature rose, and hence the tangential velocity dropped. In addition, fewer particles were trapped because of reduced centrifugal force. The largest value of separation efficiency was estimated at the lowest temperature (T=293 K), while the minimum value of separation efficiency was achieved at the highest temperature (T=700 K), which is consistent with earlier research [45]. Furthermore, the separation efficiency of all square cyclones increased as the inlet velocity increased. The increrase of tangential velocity resulted in an increased centrifugal force and particle separation efficiency [24]. When the 50% cut size was compared, it was discovered that it increased significantly as the gas temperature increased. The 50% cut size refers to the particle size at which the cyclone efficiency is 50%. [49]. At T=293 K, the 50% cut size was 17.7 μm, but it increased to 18.6 μm, which indicates an increase of 5% with v=12 m/s and particle mass loading of 41.7 g/m^3.

CONCLUSIONS

The impact of particle mass loading on the internal flow field and particle separation efficiency of the square cyclone at low and high temperatures were examined using CFD modeling. The Eulerian-Lagrangian technique was utilized to analyze the airflow and particle dynamics in the square cyclone. The CFD simulation allows for the calculation of the fine details of particle motion as well as the evaluation of separation efficiency. Particle mass loadings ranging from 6.9 to 41.7 g/m^3 were considered. The precision of CFD

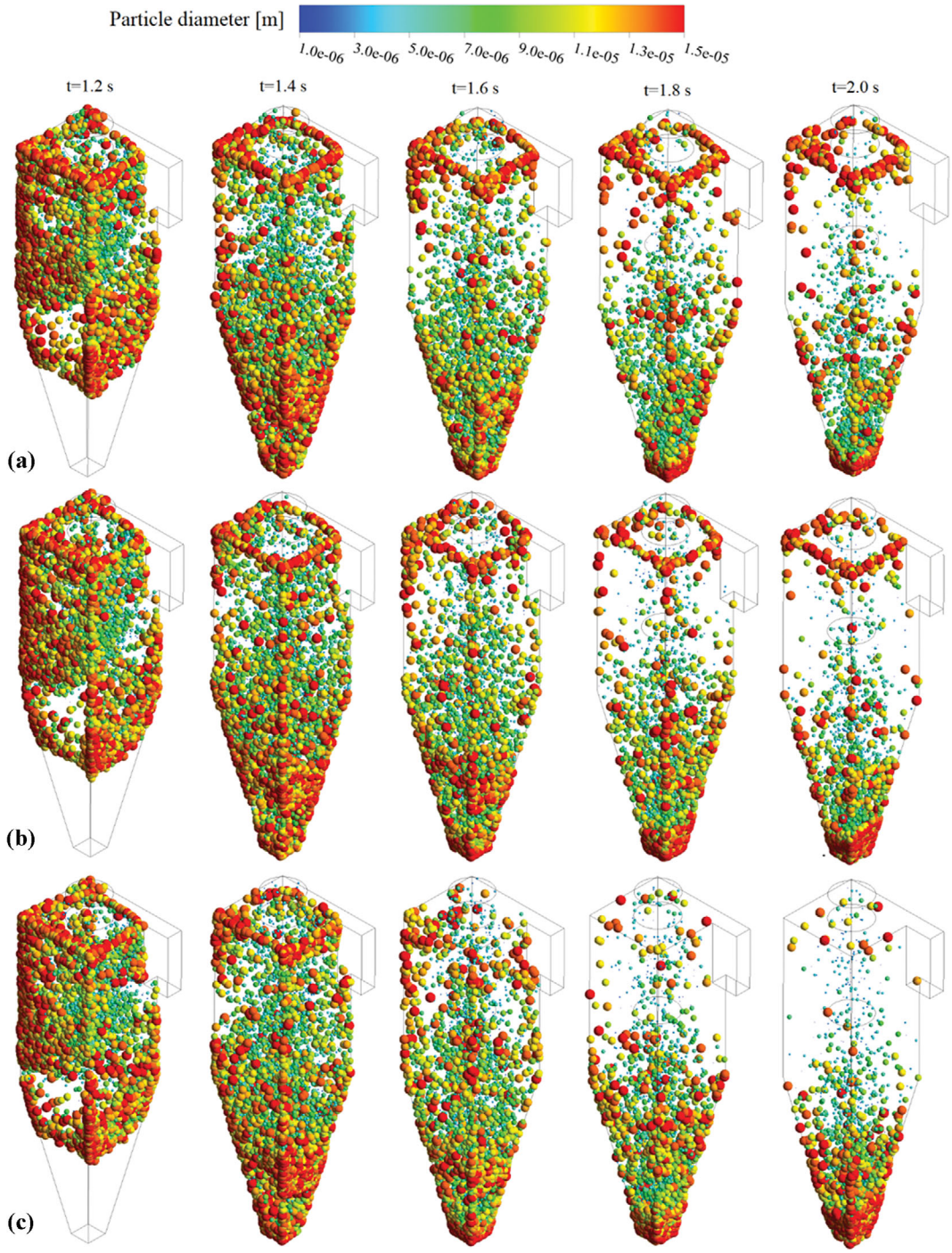

Fig. 20. Particle motion under different mass loading at v=12 m/s (a) 6.9 g/m^3 (b) 20.8 g/m^3 and (c) 41.7 g/m^3 at T=293 K.

modeling was demonstrated by comparing predicted pressure drop and separation efficiency to experimental data of ref. [25] and numerical results of ref. [3], which showed good agreement.

- The particle-laden flow in the square cyclone separator was better-understood thanks to CFD modeling.
- The flow pattern and performance of the square cyclone were impacted by both particle mass loading and gas temperature, with the effect of gas temperature being the most significant.
- By comparing the separation process of different particles, it is obvious that the larger particles (≥8 μm) were subjected to higher centrifugal force and thus separated more easily. The majority of small particles with a diameter of 3 μm escaped through the cyclone's outlet section. The centrifugal force exerted on these small particles with a diameter of 3 μm was insufficient to handle the drag force of gas.
- The separation efficiency was increased by increasing particle mass loading because of the enhancement of the larger particle sweeping effects and the agglomeration of the smaller

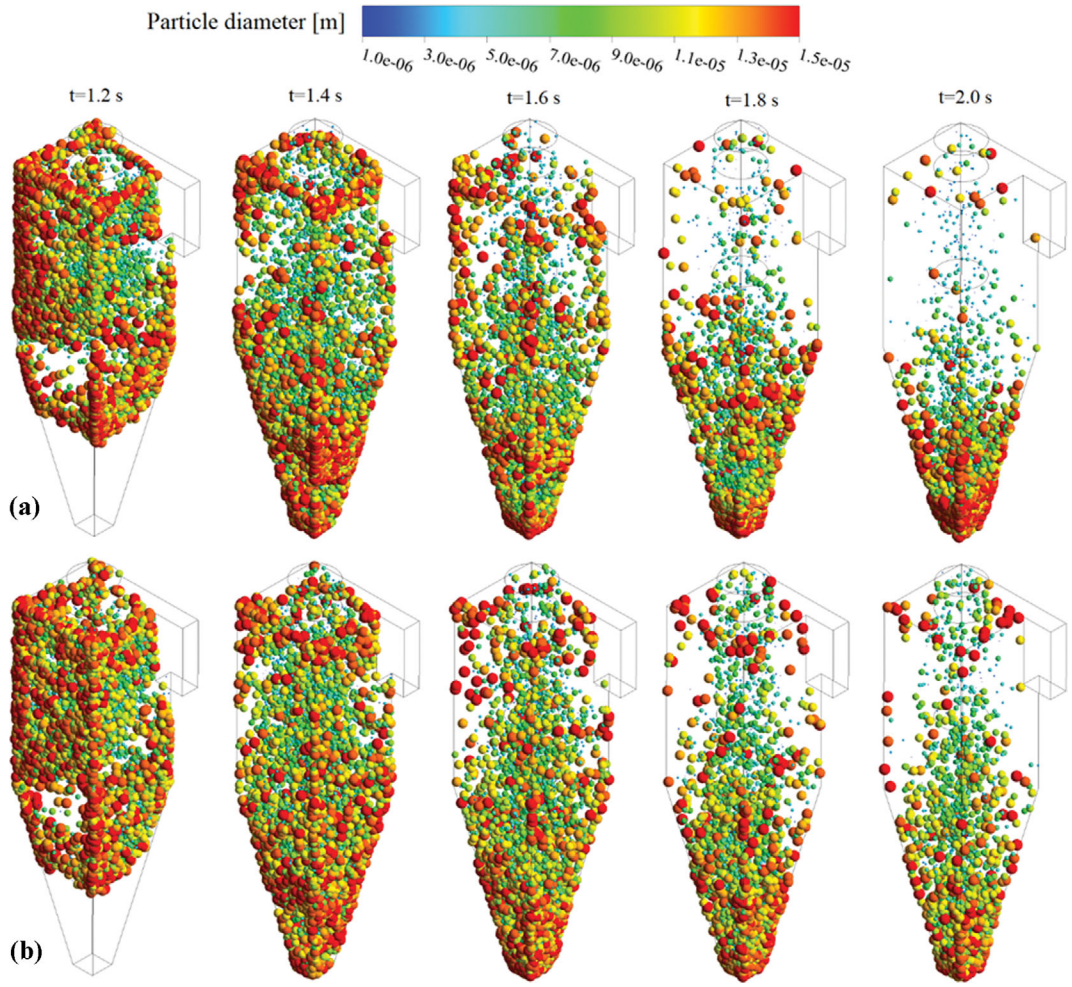

Fig. 21. Particle motion with v=12 m/s at (a) low (T=293 K) and (b) high temperatures (T=700 K).

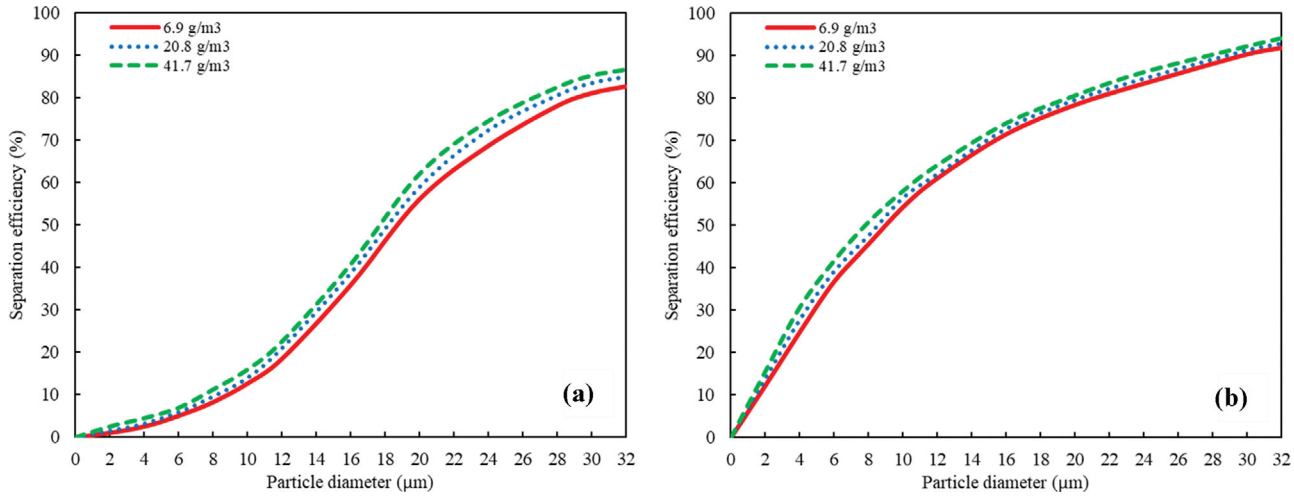

Fig. 22. Impact of particle mass loading on change of separation efficiency versus particle size at (a) v=12 m/s and (b) v=20 m/s.

particles.

- The tangential velocity was dramatically reduced when the inlet temperature was raised, resulting in a considerable loss in particle separation efficiency. Because of the reduced centrifugal force, fewer particles would be trapped.
- When the particle concentration was compared at different heights, it was found that the particle concentration was higher near the bottom since more particles were trapped with a

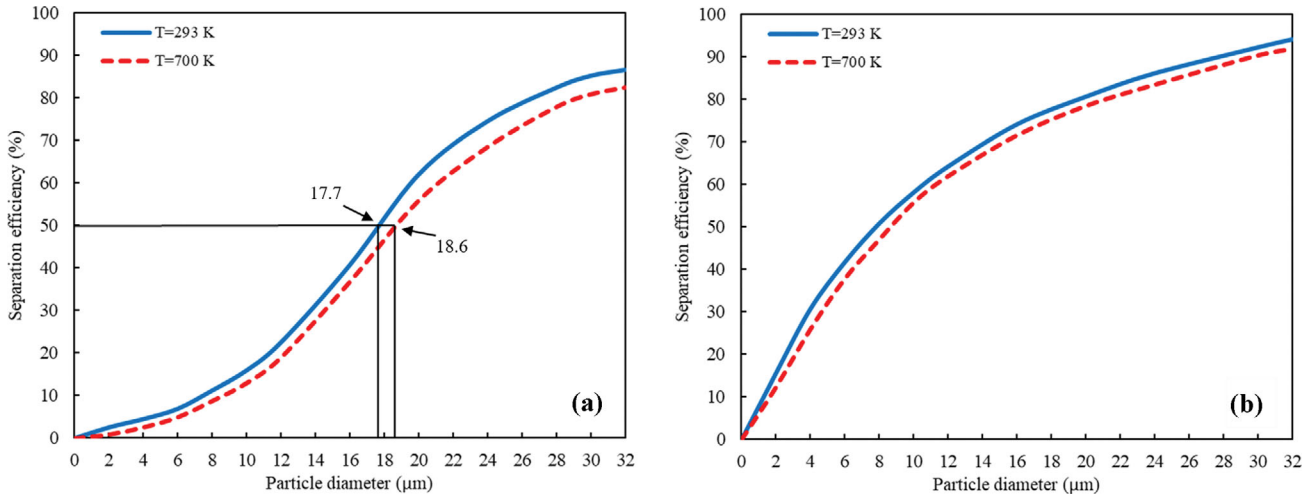

Fig. 23. Change of separation efficiency in terms of particle size (a) v=12 m/s and (b) v=20 m/s.

higher particle mass loading.

- The temperature of the gas had a greater impact than the mass of the particles. When the gas temperature was increased from 293 K to 700 K, the maximum axial velocity was lowered by 11% below the vortex finder. At the cone section near the bottom of the cyclone, the axial velocity was higher for T= 700 K, which enhanced the gas swirl flow and re-entrained the particles from the bottom.
- The observations concerning the motion of the particles which were consistent with the particle concentrations profiles demonstrated that larger particles with lower particle mass loading accumulated at the top of the main part of the cyclone so they could not be separated from the gas.
- A 5% improvement of 50% cut size was predicted with the increment of gas temperature at v=12 m/s and particle mass loading of 41.7 g/m^3.

The current study focused on the impact of particle mass loading on particle concentration and motion within a square cyclone, which was substantially influenced by particle size and gas temperature. This behavior may also happen to other forms of industrial cyclones, such as hydro-cyclones and cylindrical gas cyclones, as well as other swirling multiphase flow processes.

NOMENCLATURE

C_D : drag coefficient
ν : kinematic viscosity [m^2/s]
K : fluctuating kinetic energy [m^2/s^2]
u_i : gas velocity [m/s]
g_i : gravitational acceleration [m/s^2]
P_f : fluctuating energy production [m^2/s^3]
μ : dynamic viscosity [kg/ms]
ρ : density [kg/m^3]
ρ_p : particle density [kg/m^3]
R_{ij} : Reynolds stress tensor
u_{pi} : particle velocity [m/s]
t : time [s]
ε : turbulence dissipation rate [m^2/s^3]
v : velocity [m/s]
d_p : particle diameter [μm]
Re_p : relative Reynolds number
P : pressure [Pa]

REFERENCES

1. S. Venkatesh, M. Sakthivel, S. Sudhagar and S. A. Daniel, *Particul. Sci. Technol.*, **37**, 794 (2018).
2. O. R. Nassaj, D. Toghraie and M. Afrand, *Powder Technol.*, **356**, 353 (2019).
3. Y. Su, A. Zheng and B. Zhao, *Powder Technol.*, **210**, 293 (2011).
4. H. Fatahian and E. Fatahian, *Iran. J. Chem. Chem. Eng.*, **41**, 670 (2022).
5. E. Fatahian, H. Fatahian, E. Hosseini and G. Ahmadi, *Powder Technol.*, **387**, 454 (2021).
6. N. Malahayati, D. Darmadi, C. Putri, L. Mairiza, W. Rinaldi and Y. Yunardi, *Mater. Today-Proc.*, **63**, 318 (2022).
7. M. Wasilewski, L. Brar and G. Ligus, *Sep. Purif. Technol.*, **239**, 116588 (2020).
8. H. Safikhani, M. Akhavan-Behabadi, N. Nariman-Zadeh and M. Abadi, *Chem. Eng. Res. Des.*, **89**, 301 (2011).
9. S. Venkatesh, R. S. Kumar, S. Sivapirakasam, M. Sakthivel, D. Venkatesh and S. Arafath, *Powder Technol.*, **371**, 115 (2020).
10. M. Wasilewski, L. Brar and G. Ligus, *Sep. Purif. Technol.*, **274**, 119020 (2021).
11. S. Venkatesh, S. Sivapirakasam, M. Sakthivel, S. Ganeshkumar, M. Prabhu and M. Naveenkumar, *Powder Technol.*, **383**, 103 (2021).
12. H. Safikhani, M. Shams and S. Dashti, *Adv. Powder Technol.*, **22**, 359 (2011).
13. H. Fatahian, E. Fatahian and M. E. Nimvari, *Powder Technol.*, **339**, 232 (2018).
14. H. Fatahian, E. Hosseini and E. Fatahian, *Adv. Powder Technol.*, **31**, 1748 (2020).
15. A. Raoufi, M. Shams and H. Kanani, *Powder Technol.*, **191**, 349 (2009).

16. E. Hosseini, *J. Brazil. Soc. Mech. Sci. Eng.*, **42**, 1 (2020).
17. H. Fatahian, E. Fatahian, M. E. Nimvari and G. Ahmadi, *Powder Technol.*, **380**, 67 (2021).
18. H. Safikhani, M. Rafiee and D. Ashtiani, *Adv. Powder Technol.*, **32**, 3268 (2021).
19. J. Gimbun, T. Chuah, A. Fakhru'l-Razi and T. Choong, *Chem. Eng. Process: Process Intens.*, **44**, 7 (2005).
20. I. Karagoz and F. Kaya, *Int. Commun. Heat Mass.*, **34**, 1119 (2007).
21. M. Siadaty, S. Kheradmand and F. Ghadiri, *Adv. Powder Technol.*, **28**, 1459 (2017).
22. E. Yohana, M. Tauviqirrahman, B. Yusuf, K. H. Choi and V. Paramita, *Powder Technol.*, **377**, 464 (2021).
23. A. N. Huang, N. Maeda, S. Sunada, T. Fukasawa, H. Yoshida, H. Kuo and K. Fukui, *Sep. Purif. Technol.*, **183**, 293 (2017).
24. A. Jafarnezhad, H. Salarian, S. Kheradmand and J. Khaleghinia, *J. Brazil. Soc. Mech. Sci. Eng.*, **43**(2), 1 (2021).
25. F. Qian, Z. Huang, G. Chen and M. Zhang, *Comput. Chem. Eng.*, **31**, 1111 (2007).
26. K. W. Chu, B. Wang, D. L. Xu, Y. X. Chen and A. B. Yu, *Chem. Eng. Sci.*, **66**, 834 (2011).
27. P. Kozołub, A. Klimanek, R. Białecki and W. Adamczyk, *Particuology*, **31**, 170 (2017).
28. S. Bogodage and A. Y. Leung, *J. Hazard. Mater.*, **311**, 100 (2016).
29. A. N. Huang, K. Ito, T. Fukasawa, K. Fukui and H. Kuo, *J. Taiwan Inst. Chem. E.*, **90**, 61 (2018).
30. J. Derksen, S. Sundaresan and H. Van den Akker, *Powder Technol.*, **163**, 59 (2006).
31. G. Wan, G. Sun, X. Xue and M. Shi, *Powder Technol.*, **183**, 94 (2008).
32. Y. Su and Y. Mao, *Chem. Eng. J.*, **121**, 51 (2006).
33. K. Elsayed and C. Lacor, *Powder Technol.*, **217**, 84 (2012).
34. K. Elsayed and C. Lacor, *Appl. Math. Model.*, **35**, 1952 (2011).
35. S. Bogodage and A. Y. Leung, *Powder Technol.*, **286**, 488 (2015).
36. B. Launder, G. Reece and W. Rodi, *J. Fluid Mech.*, **68**, 537 (1975).
37. A. J. Hoekstra, J. Derksen and H. Van Den Akker, *Chem. Eng. Sci.*, **54**, 2055 (1999).
38. K. Elsayed and C. Lacor, *Chem. Eng. Sci.*, **65**, 6048 (2010).
39. H. Safikhani, A. Hajiloo and M. Ranjbar, *Comput. Chem. Eng.*, **35**, 1064 (2011).
40. K. Elsayed and C. Lacor, *Comput. Fluids*, **68**, 134 (2012).
41. S. A. Morsi and A. J. Alexander, *J. Fluid Mech.*, **55**, 193 (1972).
42. K. Elsayed and C. Lacor, *Comput. Fluids*, **51**, 48 (2011).
43. F. Parvaz, S. Hosseini, K. Elsayed and G. Ahmadi, *Sep. Purif. Technol.*, **201**, 223 (2018).
44. C. Song, B. Pei, M. Jiang, B. Wang, D. Xu and Y. Chen, *Powder Technol.*, **294**, 437 (2016).
45. E. Hosseini, H. Fatahian, G. Ahmadi, M. Eshagh Nimvari and E. Fatahian, *J. Brazil. Soc. Mech. Sci. Eng.*, **43**(9), 1 (2021).
46. M. Wasilewski and L. Brar, *Sep. Purif. Technol.*, **213**, 19 (2019).
47. M. Shin, H. Kim, D. Jang, J. Chung and M. Bohnet, *Appl. Therm. Eng.*, **25**, 1821 (2005).
48. M. Siadaty, S. Kheradmand and F. Ghadiri, *Appl. Therm. Eng.*, **137**, 329 (2018).
49. H. Erol, O. Turgut and R. Unal, *Heat Mass Transfer*, **55**, 2341 (2019).
50. S. Wang, H. Li, R. Wang, X. Wang, R. Tian and Q. Sun, *Adv. Powder Technol.*, **30**, 227 (2019).
51. Y. Wakizono, T. Maeda, K. Fukui and H. Yoshida, *Sep. Purif. Technol.*, **141**, 84 (2015).
52. F. Qian, Z. Huang, G. Chen and M. Zhang, *Comput. Chem. Eng.*, **31**, 1111 (2007).